The zinc efflux activator SczA protects *Streptococcus pneumoniae* serotype 2 D39 from intracellular zinc toxicity

Julia E. Martin[1,5], Katherine A. Edmonds[1,5], Kevin E. Bruce[2], Gregory C. Campanello[1,3], Bart A. Eijkelkamp[4], Erin B. Brazel[4], Christopher A. McDevitt[4], Malcolm E. Winkler[2], and David P. Giedroc[1]#

[1]Department of Chemistry, Indiana University, Bloomington, IN 47405-7102 USA; [2]Department of Biology, Indiana University, Bloomington, IN 47405-7005 USA; [3]Present address: Department of Biological Chemistry, University of Michigan Medical School, Ann Arbor, MI 48109 USA; [4]Research Centre for Infectious Diseases, School of Biological Sciences, the University of Adelaide, SA, Australia 5005; [5]These authors contributed equally to this work.

#Corresponding author: (812) 856-3178; fax (812) 856-5710; giedroc@indiana.edu

Running Title: Functional determinants of the pneumococcal zinc efflux regulator SczA

This is the author manuscript accepted for publication and has undergone full peer review but has not been through the copyediting, typesetting, pagination and proofreading process, which may lead to differences between this version and the Version record. Please cite this article as doi:10.1111/mmi.13654.

Abstract

Zinc is an essential trace element that serves as a catalytic cofactor in metalloenzymes and a structural element in proteins involved in general metabolism and cellular defenses of pathogenic bacteria. Despite its importance, high zinc levels can impair cellular processes, inhibiting growth of many pathogenic bacteria, including the major respiratory pathogen *Streptococcus pneumoniae*. Zinc intoxication is prevented in *S. pneumoniae* by expression of the zinc exporter CzcD, whose expression is activated by the novel TetR-family transcriptional zinc-sensing regulator SczA. How zinc bioavailability triggers activation of SczA is unknown. We show here through functional studies in *S. pneumoniae* that an unannotated homodimeric TetR from *S. agalactiae* (PDB 3KKC) is the *bona fide* zinc efflux regulator SczA, and binds two zinc ions per protomer. Mutagenesis analysis reveals two metal binding sites, termed A and B, located on opposite sides of the SczA C-terminal regulatory domain. *In vivo*, the A- and B-site SczA mutant variants impact *S. pneumoniae* resistance to zinc toxicity and survival in infected macrophages. We propose a model for *S. pneumoniae* SczA function in which both A- and B-sites are required for transcriptional activation of *czcD* expression, with the A-site serving as the evolutionarily conserved intracellular sensing site in SczAs.

Introduction

Zinc (Zn) is an essential trace element for all organisms (Andreini *et al.*, 2006). It serves as a required catalytic cofactor for a wide and functionally diverse range of enzymes, including hydrolytic enzymes, *e.g.,* metallopeptidases, esterases, and alcohol dehydrogenases (McCall *et al.*, 2000). Zn is also required in a large number of significantly important metabolic regulatory proteins as a structural component, in helping to maintain protein stability. Given the importance of Zn in general metabolism and cellular defenses (Djoko *et al.*, 2015; Bonaventura *et al.*, 2015), it is understandable that imbalances in Zn homeostasis can impair fitness of organisms. Thus, there is an exquisite need to tightly control intracellular Zn levels and bioavailable (readily accessible) Zn stores.

In mammals, total associated Zn levels vary significantly among tissue sites (≈100-650 μM) (McDevitt *et al.*, 2011). During inflammation, these Zn levels can rise, resulting in activation and recruitment of various immune cells to specific host sites of infection (Milanino *et al.*, 1993; Botella *et al.*, 2011; Ong *et al.*, 2014). The concentration of bioavailable Zn at these sites has yet to be accurately measured by available methods. However, it has been demonstrated that approximately 15% of the total associated Zn in the airway mucosal epithelium is bioavailable (Zalewski *et al.*, 2005). In any case, it is well known that elevated Zn levels can inhibit metabolic processes and virulence pathways in bacteria (Djoko *et al.*, 2015), including the major human respiratory pathogen *Streptococcus pneumoniae* (Eijkelkamp *et al.*, 2014; McDevitt *et al.*, 2011), and this is an important component of the host-pathogen interface (Capdevila *et al.*, 2016; Nairn *et al.*, 2016).

Excessively high intracellular Zn levels are prevented by inducing the expression of proteins that mediate Zn efflux. These proteins include members of the ZIP, P-type ATPase,

resistance nodulation division pumps (RND), and cation diffusion facilitator (CDF) families (Hantke, 2001). For several bacteria, including *S. pneumoniae*, the CDF family metal/H^+ antiporter CzcD serves as the major Zn-resistance determinant (Anton *et al.*, 1999; Jacobsen *et al.*, 2011; Kloosterman *et al.*, 2007; Martin and Giedroc, 2016). Deletion of *czcD* reduces virulence of bacterial pathogens and renders *S. pyogenes* more susceptible to polymorphonuclear leucocyte killing (Ong *et al.*, 2015; Ong *et al.*, 2014).

Transcription of *czcD* is regulated by the novel tetracycline repressor (TetR) family response factor SczA, which is believed to exhibit dual functionality in *S. pneumoniae*, as both a repressor and an activator of transcription by sensing intracellular Zn levels (Fig. 1) (Kloosterman *et al.*, 2007). When Zn is limited, SczA binds a palindromic conserved DNA sequence adjacent to the consensus sequences for RNA polymerase recruitment and represses *czcD* transcription (Fig. 1B) (Kloosterman *et al.*, 2007). When Zn is in excess, SczA occupies a different site upstream in the *czcD* promoter, mediating induction of CzcD expression, thereby increasing Zn efflux (Fig. 1B) (Kloosterman *et al.*, 2007). The mechanism that leads to this switch in DNA-binding site occupancy and which metal-binding residues are required for activation of SczA are unknown.

The TetR family of proteins collectively interact with a wide array of ligands and regulate many cellular processes. Canonical TetRs mediate cellular resistance to toxic antibiotics or lipophilic compounds and up-regulate the expression of downstream genes, generally via ligand-mediated transcriptional derepression, encoding proteins that are responsible for efflux of these toxic compounds (Cuthbertson and Nodwell, 2013). SczA is unique as the first identified metal-sensing regulatory protein of the TetR family, and also fails to conform to the general paradigm of ligand-mediated transcriptional depression, since SczA activates transcription of an efflux

pump to prevent cellular Zn toxicity. Despite the extraordinary functional diversity of the TetR family, the structural features include many commonalities. TetR-family repressors adopt a homodimeric architecture composed of two domains (Fig. 2): a highly conserved N-terminal DNA-binding domain (α1-α3) consisting of a helix-turn-helix motif with the α1 helix typically preceded by a positively charged region that makes contacts with the DNA minor groove; and a variable C-terminal regulatory domain (α4-α9) that is involved in dimerization and ligand binding (Cuthbertson and Nodwell, 2013). Helices α5-α7 form a central "triangle" outlining a ligand-binding cavity that may be accessible from the front, side, or top of the molecule when oriented with the DNA binding domains pointing down (see Fig. 2), depending on the specific TetR-family protein member (Cuthbertson and Nodwell, 2013).

In this work, we identify a second TetR-family SczA from *S. agalactiae* 2603 serotype V exhibiting 48% sequence identity to the *S. pneumoniae* D39 serotype 2 SczA. Through an extensive sequence analysis of *Streptococcus* spp., and metal-binding and phenotypic growth analysis, we identify several determinants required for Zn-dependent activation of SczA. Our *in vivo* and *in vitro* functional analysis of SczA in *S. pneumoniae* and *S. agalactiae* provide new insights into how this novel TetR-family response factor senses intracellular Zn bioavailability, thereby activating SczA and upregulating *czcD* transcription.

Results

S. agalactiae gene locus tag SAG0431 encodes a *bona fide* SczA

An unannotated TetR-family protein from *S. agalactiae* 2603 serotype V (gene locus tag SAG0431) deposited by the Midwest Center for Structural Genomics in the Protein Data Bank (PDB code 3KKC) exhibits 48% amino-acid sequence identity to *S. pneumoniae* D39 serotype 2 SczA (Fig. 3; see Fig. S1 for the extended alignment). The structure shows one metal ion per protomer, annotated as a nickel ion (Ni(II)), coordinated by a histidine triad of H68, H84 and H88 (the *S. pneumoniae* amino acid numbering system is used consistently throughout this paper for simplicity) and three additional ligands from solvent. Although Ni(II) is reported to activate *czcD* transcription in *S. pneumoniae*, Ni(II) is unlikely to be physiologically relevant in *S. pneumoniae* as only trace amounts are found associated with pneumococcal cells (Kloosterman *et al.*, 2007) and there are no known Ni(II)-requiring enzymes expressed by *S. pneumoniae*.

Based on protein sequence and genomic context similarities, *i.e.*, both genes are located in a divergently transcribed operon associated with a CDF efflux transporter, we hypothesized that SAG0431 might perform the same biological function as SczA in *S. pneumoniae*. To test this, we first constructed a *sczA*-null *S. pneumoniae* D39 strain and compared its functional properties with a *czcD*-null mutant that is unable to export Zn out of the cytoplasm. Consistent with previous studies (Bijlsma *et al.*, 2007; Martin and Giedroc, 2016; Jacobsen *et al.*, 2011), a rich growth medium supplemented with 300 μM Zn perturbs pneumococcal growth of cells lacking *czcD* or *sczA* (Figs. 4 and S2). This growth phenotype is rescued by allelic replacement with a C-terminally FLAG-tagged *S. pneumoniae* SczA or *S. agalactiae* SAG0431 (Figs. 4 and S2). The minor difference in growth yields between SAG0431 and *S. pneumoniae* SczA complementation may be attributed to differences in protein sequence identity or possibly

operator sequence recognition. However, as SAG0431 complemented the *S. pneumoniae sczA*-null mutant, these data indicate that the protein product of SAG0431 is an orthologous SczA.

***S. pneumoniae* SczA and *S. agalactiae* SczA harbor two metal-binding sites per protomer**

Although Ni(II) is refined in the crystal structure of *S. agalactiae* SczA and may be capable of modulating the binding of *S. pneumoniae* SczA to the *czcD* promoter *in vitro* (Kloosterman *et al.*, 2007), Zn(II) is expected to be the physiologically relevant activator of *czcD* expression. Moreover, given the physical properties of Ni(II) and Zn(II), Zn(II) may bind to SczA differently than the Ni(II) in the structure. We therefore sought to explore Zn(II) binding to SczA *in vitro*. To our surprise, we found that purified apo *S. pneumoniae* SczA binds two Zn(II) ions per protomer, or 4 per homodimer, at pH 8.0 in competition with a modest affinity competitor chelator, mag-fura-2 (mf2) (Fig. 5A). One of the binding sites has high affinity, with an association equilibrium (K_{Me}) constant above that measurable by competition with mf2 (log $K_{Zn1}\geq 9$), while the other is of more modest affinity (log K_{Zn2} 7.9±0.1). Zn(II) binding to *S. pneumoniae* apo-SczA is significantly weakened at pH 6.0 (log K_{Zn1} 7.3±2.9 and log K_{Zn2} 4.9±0.1) (Fig. 5B), with mf2 outcompeting apo-SczA for binding of both Zn(II) ions. Although the presence of a second metal-binding site was unexpected, the strong pH-dependence is consistent with the Zn-histidine ligation in both sites, as observed in the *S. agalactiae* SczA structure (Fig. 2). We note that these metal binding experiments were hampered by the tendency of *S. pneumoniae* SczA to aggregate in solution. Therefore, further metal binding experiments were pursued *in vitro* using only *S. agalactiae* SczA. *S. agalactiae* SczA shows a similar pattern to that of the *S. pneumoniae* SczA protein, binding to two Zn(II) ions per protomer, with one

high-affinity site and one moderate affinity site (log K_{Zn1}≥9 and log K_{Zn2} 8.4±0.1, respectively) (Fig. 5C).

The metal-binding stoichiometry of wild-type *S. agalactiae* SczA was further confirmed by titrations of the apo-protein with Co(II) (Fig. 6). Co(II) is commonly used as a spectroscopically useful surrogate for Zn(II)-binding proteins since it typically adopts the same coordination geometry of the cognate metal Zn(II) (Pennella *et al.*, 2003). Our data indicate that there are two spectroscopically distinct metal-binding sites present in wild-type SczA, each with distinguishable affinities, given the distinct spectral features of the first and second molar equivalents of Co(II) added to apo-SczA (Fig. 6A). The high affinity Co(II)-site adopts a high-coordination number complex (ε_{max}≤20 M^{-1} cm^{-1} at ≈500 nm), likely octahedral, while the lower affinity Co(II) site appears to be tetrahedral, given the ε_{max}≈300 M^{-1} cm^{-1} at 560 nm. Neither metal-binding site is characterized by cysteine thiolate ligation, based on the lack of appreciable absorption in the near UV-region (Fig. 6A), thus revealing that C62, the only cysteine in SczA (see Fig. 3), is not recruited into either metal chelate. Titration of Zn(II) into the Co(II)-loaded wild-type SczA protein shows Zn(II) displacement of Co(II) from the tetrahedral site first (Fig. 6B). SczA protein precipitation begins to occur prior to Zn(II) filling the octahedral site. Together, these data strongly suggest that there are two distinct metal-binding sites present in SczA that may contribute to allosteric activation of DNA operator binding (Fig. 1).

Having confirmed the presence of a second metal-binding site in SczA, we sought to identify it in the structure. We reasoned that the high-affinity Co(II) site likely corresponds to the octahedral site A identified in the crystal structure bound to Ni(II), while the lower-affinity Co(II) site corresponds to a site B elsewhere in the protein. Comparative sequence alignments of SczA candidates from other streptococci was performed to identify other conserved potential

metal binding residues in the ligand-binding core of SczA (α5-α7), in particular histidines. We observed that SczA proteins exhibit a second cluster of conserved potential metal-binding residues, designated here as site B, including H67 in the α4 helix and E114, E116, H117, and H118 in the α7 helix (see Figs. 3 and S1), near the Ni(II)-site in the C-terminal regulatory domain in the *S. agalactiae* SczA structure (Fig. 2). The structure suggests that E114, H117, and H118 are well-poised to coordinate a metal, while some structural rearrangement might be necessary to accommodate coordination by H67 or E116, the latter of which clearly points away from the E114, H117 and H118 in the structure (Fig. 2).

Residues R6 and K10 are required for SczA function

The DNA-binding domains of TetR-family proteins are composed of N-terminal helices α1-α3 (Fig. 3). Based on a number of structures of TetR protein-DNA complexes, α3 serves as the DNA recognition helix, forming specific contacts with the DNA major groove, while α1 and an N-terminal extension often make contacts with the DNA minor groove, immediately flanking major groove recognition determinants (Le *et al.*, 2011; Orth *et al.*, 2000; Schumacher *et al.*, 2002). Positively charged residues, particularly arginine and lysine, typically mediate these contacts. Our sequence alignment (Fig. S1) shows that R6 and K10 in the N-terminal region are well-conserved and may contribute to SczA function. Pneumococcal strains harboring amino acid substitutions of R6 and K10 with a non-charged alanine residue in SczA fail to grow in the presence of Zn-stress (Fig. 7A and S2), despite wild-type levels of expression of SczA (Fig. S3). ICP-MS shows that these mutant strains accumulate ≈2-fold more cell-associated Zn than wild-type (WT) cells during Zn stress (Fig. 7B, *grey* bars), suggesting that R6A and K10A SczA variants are unable to induce *czcD* transcription. Indeed, no CzcD protein was detected by

western blots during Zn-stress (Fig. S4). *In vitro* metal-binding spectroscopic analysis shows that both SczA-R6A and SczA-K10A retain two metal-binding sites like WT-SczA (Fig. 6E), suggesting that these mutations within the DNA-binding domain of SczA do not affect metal-binding events in the C-terminal regulatory domain, and most likely affect SczA-DNA binding complex formation.

The crystal structure of *Sag* SczA shows residues R6 and K10 as part of an unusually extended α1 helix, raising questions as to how they could make significant contacts to the DNA phosphate backbone as previously observed in structures where the basic residues are in flexible regions N-terminal to α1. The extended helix would force R6 to point away from the DNA (Fig. 2); however, it is also possible that α1 is lengthened in the structure by a crystal-packing artifact. Although the solution structure of apo-SczA is beyond the scope of this work, analysis by nuclear magnetic resonance spectroscopy (NMR) shows that R6 and K10 are indeed in an unstructured, highly flexible N-terminal region, outside of the α1 helix in solution (Fig. S5). The assigned chemical shifts of residues 1-10 are not consistent with helical geometry; in contrast, these residues have low ^{15}N-{^{1}H}-heteronuclear NOEs, reflective of a non-helical, highly dynamic region of the protein (Fig. S5). Thus, the available structural data support the notion that residues R6 and K10 are vital to the function of SczA, likely due to their ability to enhance DNA binding through contacts with the phosphate backbone.

The octahedral coordinating metal-binding site A is required for activation of SczA

The Ni(II)-bound *S. agalactiae* SczA structure predicts that invariant residues H68 in the α4 helix and H84 and H88 in α5 are metal binding ligands (see site A; Fig. 2). *In vitro* *s*pectroscopic analysis using our Co(II) titration assay confirms that these three residues

physically coordinate a single metal ion with octahedral coordination geometry (Fig. 8A), since amino acid single or double substitutions of these residues with alanine results in the specific loss of the octahedral binding event ($\varepsilon_{max} \leq 20$ M^{-1} cm^{-1} at ≈500 nm), but retention of the tetrahedral binding event in all cases (Fig. 6C) relative to WT SczA (Fig. 6A).

In vivo, we find that a H68A substitution in *S. pneumoniae* SczA increases Zn sensitivity (Fig. 7A and S2) and Zn accumulation relative to WT cells during Zn stress (Fig. 7B, *grey* bars). A modest growth defect is observed for the H84A mutants, while the H88A mutants grew similar to WT cells when stressed when Zn (Fig. 7A and S2). WT-like cell-associated Zn concentrations are observed for both H84A and H88A variant strains independent of Zn stress (Fig. 7B). CzcD expression was significantly lower in cells expressing SczA-H84A (Fig. S4), but sufficient to prevent significant cellular Zn toxicity. Interestingly, a strain harboring the double mutant H84A/H88A SczA fails to grow during Zn-stress (Fig. 7A), despite being expressed at a level exceeding that of WT-SczA (Fig. S3B). A 2.5-fold increase in Zn accumulation is associated with the SczA-H84A/H88A mutant strain, relative to WT, in the presence of Zn stress (Fig. 7B), a finding consistent with undetectable levels of CzcD protein by western blot (Fig. S4). These data confirm that the single SczA-H84A and SczA-H88A mutant proteins are only partially functional. Together, these data strongly suggest that H68 and likely, H84 and H88, physically coordinate Zn(II) in site A (Fig. 8A) and each is important for transcriptional activation of *czcD* expression by SczA. If one assumes that coordination numbers for Zn(II) and Co(II) at site A are the same, then the octahedral coordination geometry may very well involve the recruitment of one or more ligands from the solvent.

The tetrahedral coordinating metal-site B is important for SczA function

We next evaluated the composition and significance of site B in SczA. *In vitro* spectroscopic analysis of B-site SczA mutant proteins including H67A, E114A, E116A, H117A, and H118A mutants, reveals a specific loss of tetrahedral coordination of Co(II) for all mutants tested (no ε_{max}≈300 M^{-1} cm^{-1} at 560 nm) (Fig. 6D), with the exception of E116A SczA (Fig. 6E), when compared to the WT SczA (Fig. 6A). The Co(II) titration spectra for E116A SczA (Fig. 6E, third panel) track those of WT SczA (Fig. 6A), displaying two independent metal-binding coordination events with Co(II). Substitution of D118 with cysteine (D118C) retains the signature strong peaks indicative of tetrahedral geometry, but with an intense and increased absorption in the near UV-region, indicative of cysteine-thiolate ligation to Co(II) in the metal-binding site B (Fig. 6F). These data show that D118 is a direct ligand in the metal chelate, while H67, E114 and H117 are also important and likely coordinate the metal ion with tetrahedral coordination geometry in site B of SczA (Fig. 8A).

In vivo mutational analysis of B-site residues further reveals that strains harboring alanine substitutions of H67, E114, E116, H117, and H118 show variable growth phenotypes compared to WT *S. pneumoniae* strain during zinc stress (Fig. 7A, *grey* bars and Fig. S2) but show similar WT-like growth pattern when not stressed (Fig. 7A, *black* bars). We find that pneumococcal cells expressing H67A SczA or H118A SczA fail to grow in the presence of Zn stress, whereas the E114A SczA variant shows only a modest growth defect relative to WT cells (Fig. 7A). Strains encoding the E116A SczA and, to our surprise, the H117A SczA variant, are characterized by WT-like growth yields independent of Zn stress (Fig. 7A). Cell-associated Zn levels are consistent with growth phenotypes, in which H67A and H118A SczA mutants accumulate ≈2-fold more Zn than WT cells during Zn stress (Fig, 8B, *grey* bars). A slight increase in Zn is observed for E114A SczA mutant, while the E116A and H117A SczA strains

possess WT-like cellular Zn levels when grown with excess Zn (Fig. 7B). We show that all SczA constructs are expressed at or near WT-like levels (Fig. S3) and that CzcD protein was only detected in the E116A and H117A SczA mutant strains by western blot (Fig. S4). The latter are consistent with a functional SczA. Taken together, these data suggest that site B comprises residues H67, E114, and H118, which coordinate the metal in a tetrahedral coordination geometry (Fig. 8A) and contribute to SczA function *in vivo*. The observation that H117 is required for tetrahedral Co(II) binding *in vitro*, yet dispensable for response to Zn(II) stress *in vivo*, suggests either that there are differences in the B-site coordination complexes between Co(II) and Zn(II), or the functional impact of a single H117A mutant in the site B is smaller relative to the other residues.

SczA mutants show decreased survival in mammalian-host macrophages

Emerging evidence suggests that mammalian host cells are capable of exploiting Zn toxicity to kill invading pathogenic bacteria (Djoko *et al.*, 2015; Bonaventura *et al.*, 2015; Ong *et al.*, 2014). Several reports have demonstrated that CzcD is essential for resistance against Zn-killing by neutrophils and that streptococci lacking *czcD* are hypersensitive to polymorphonuclear leucocyte killing, indicating that CzcD is important for virulence (Ong *et al.*, 2015; Ong *et al.*, 2014). Here, we show that the survival *S. pneumoniae sczA*-null mutants is severely compromised in human THP1-derived macrophages (Fig. 9), suggesting that these bacteria are susceptible to intramacrophage Zn toxicity, similar to the impact observed in *in vitro* liquid culture experiments (Fig. 7A).

We next assessed the ability of SczA mutant strains to survive in this Zn-intoxicating microenvironment. We find that the N-terminal positively-charged amino acid substitution

mutants (R6A and K10A) show significantly reduced survival in human macrophages relative to WT cells (Fig. 9). We also find that mutations in the A-site (H68A or H84A/H88A) that show poor induction of *czcD* in liquid culture have significantly reduced survival rates, whereas single mutants *sczA*-H84A and *sczA*-H88A are not statistically different relative to WT (Fig. 9), a finding consistent with the liquid culture results. Site B mutant strains also follow a trend similar to that observed for growth and metal analysis in liquid culture. Here, pneumococcal cells expressing H67A or H118A SczAs show clearly reduced survival rates relative to the WT strain, consistent with these residues functioning as anchoring ligands to the B-site metal (Fig. 8A). In contrast, the *sczA*-E114A strain is essentially wild-type, while the *sczA*-E116A, and *sczA*-H117A mutants give modestly impaired resistance to intramacrophage Zn toxicity and clearance (Fig. 9).

Taken together, these data demonstrate that R6 and K10 in the α1 helix of the DNA-binding domain, and that both A and B metal-binding sites found in the C-terminal regulatory domain of SczA are significantly important in dictating an *in vivo* resistance to Zn toxicity in the context of a true host-induced antimicrobial Zn stress model. This resistance correlates with the ability of SczA to function as a Zn-induced transcriptional activator of *czcD* expression.

The bioavailable Mn/Zn ratio affects CzcD expression

Accumulating evidence indicates that Zn and manganese (Mn) homeostasis are interconnected in *S. pneumoniae* (Eijkelkamp *et al.*, 2014; Imlay, 2014; Honsa *et al.*, 2013; Jacobsen *et al.*, 2011) and that the Mn/Zn ratio may dictate the specific activities of enzymes and regulatory proteins inside cells (Martin *et al.*, 2017). For example, high extracellular Zn concentrations can impose Mn limitation by binding to the high-affinity Mn solute-binding protein PsaA of the PsaBCA Mn-specific importer, forming a stable Zn-protein complex that

prohibits Zn release, rendering the PsaBCA importer nonfunctional (Counago *et al.*, 2014). Furthermore, Zn can outcompete Mn for binding to the Mn-response DtxR-family repressor PsaR, forming a PsaR:2 Zn(II) complex that represses *psaBCA* transcription, thereby reducing Mn import (Lisher *et al.*, 2013; Kloosterman *et al.*, 2008). Mn limitation, on the other hand, has been shown to induce *czcD* transcription resulting in lower cell-associated Zn levels (Ogunniyi *et al.*, 2010), while Mn intoxication increases Zn levels by 2-fold (Martin *et al.*, 2017). Together, these data suggest to us that Mn might play a role in SczA activation, possibly acting as an antagonist analogous to the ability of Zn to antagonize PsaR function (Lisher *et al.*, 2013).

To test the effect of the bioavailable Mn/Zn ratio on SczA function, we grew WT cells in a BHI growth medium with or without Mn, stressed these cells with increasing concentrations of Zn, and measured CzcD protein expression by western blot. As described above, addition of Zn (≥100 μM) to the BHI growth medium induces CzcD expression in WT pneumococcal cells (Fig. 10A) via Zn activation of SczA. Pre-adaption of WT cells with 200 μM Mn significantly reduces the level of CzcD expression that occurs upon addition of Zn stress, relative to growing the cells without excess Mn (Figs. 10A and S6). Similar CzcD expression patterns are also observed for pneumococcal cells lacking the Mn-specific CDF exporter MntE (Fig. 10B), which has been previously shown to accumulate 2-fold more Mn relative to WT cells (Martin and Giedroc, 2016); increasing Zn-stress leads to increased CzcD protein levels in *mntE*-null mutants. However, the degree of CzcD expression in the *mntE*-null mutant is ≈2-fold lower than that found in WT cells stressed with Zn (Fig. 10A-B, *black* bars). CzcD protein levels are reduced even further when *mntE*-null mutants are pre-grown with Mn (Fig. 10B, *grey* bars). These data suggest that the bioavailable Mn/Zn ratio plays a role in SczA activation and that Mn may possibly bind directly to SczA, antagonizing its function.

To test for direct binding of Mn to SczA *in vitro*, we first evaluated mf2 competition. The cell-associated Mn to Zn ratio is equal to ≈1 in *S. pneumoniae* (Martin *et al.*, 2017); however, the actual intracellular Mn and Zn concentrations are not known and intracellular Mn concentrations may be much higher than that of Zn. Given this, we predicted that Mn might bind SczA weakly in comparison to Zn. Indeed, we find that mf2 outcompetes apo-SczA for binding of Mn(II) ions, providing only an upper limit on the affinity of log K_{Mn}<4 (Fig. S7). Since affinities for Mn(II) of this magnitude may still be physiologically relevant, we next explored whether Mn binds site-specifically to SczA *in vitro* by NMR. Although large proteins can be challenging to study by NMR spectroscopy, we were able to obtain the sequence-specific residue assignments of the backbone atoms of uniformly ^{2}H,^{13}C,^{15}N apo-SczA (42 kDa dimer) (red contours in Fig. S8). Because Mn(II) is paramagnetic, addition of Mn(II) to an NMR sample would be expected to cause line broadening and lower peak intensities. Indeed, addition of Mn(II) to apo-SczA causes many peaks in the ^{15}N TROSY spectrum to vanish entirely, while others are severely diminished (blue contours in Fig. S7). Although all signals are weaker with the addition of equimolar Mn(II) (Fig. 10C), peaks remain for both the DNA-binding domain (α1- α3) and for the dimerization helices (α8-α9), but are largely obliterated in the metal-binding helices α4-α7, suggesting that Mn is coordinated by residues closest to the mapped metal-binding sites. The spatial pattern is particularly clear when plotted onto the structure (Fig. 10D). Unfortunately, the paramagnetic broadening induced by Mn(II) is such that the spatial resolution is insufficient to determine whether Mn(II) binds to site A, site B, or both. Despite this, these data demonstrate that Mn binds specifically to the ligand-binding domain of SczA, where it antagonizes the Zn-activation function of the regulator.

Discussion

This work provides the first *in vivo* functional analysis of the novel TetR-family response factor SczA expressed by *S. pneumoniae* D39 that is conserved among *Streptococcus* spp. (Fig. S1). We show that the protein product encoded by *S. agalactiae* gene locus SAG0431 is capable of complementing a *S. pneumoniae sczA*-null strain, revealing that SAG0431, like *S. pneumoniae* SczA, is a Zn-responsive activator of *czcD* transcription. We also show that the highly conserved N-terminal residues R6 and K10 in *S. pneumoniae* are essential for SczA function in protecting pneumococcal cells from Zn toxicity, both in liquid culture and inside human macrophages. Similarity to other TetR-family regulators suggests that R6 and K10 facilitate SczA activation of *czcD* transcription by directly stabilizing the SczA-DNA binding complex. We cannot, however, exclude the remote possibility that R6 and K10 impact allosteric communication between Zn(II) binding and a physical interaction with RNA polymerase that might lead to transcriptional activation.

Structural data indicate that *S. agalactiae* SczA harbors at least one metal-binding site, designated site A here, in which one Ni(II) ion is coordinated by three histidines (H68, H84, and H88 in the *S. pneumoniae* sequence) (Fig. 2). We show that only the most N-terminal His (H68) is absolutely required to mitigate the effects of cellular Zn toxicity in both liquid culture and within the intramacrophage microenvironment. In contrast, the two C-terminal α5 helix Ni(II)-binding ligands (H84 and H88) appear to play a less important role in determining Zn resistance, since a similar effect is observed only when both H84 and H88 are substituted with alanines. This dichotomy of function, observed previously for the Zn(II)-sensing site of the ArsR-family efflux repressor CzrA from *Staphylococcus aureus* (Pennella *et al.*, 2006), reveals that H68 in α4 may be required for allosteric activation of *czcD* transcription, while the more C-terminal His

pair (H84 and H88) may simply enhance Zn affinity that leads to *czcD* transcriptional activation in cells.

Our studies also clearly reveal a second metal binding site, designated here as site B, in both *S. pneumoniae* and *S. agalactiae* SczAs that is predicted to be comprised of residues H67, E114, H117, and H118, derived from α4 and α7 helices, on the opposite side of the molecule from the previously identified Ni(II)-binding site A (Fig. 2). The *sczA*-H67A and *sczA*-H118A strains that target site B give rise to a strong growth phenotype in both liquid culture and within the intramacrophage microenvironment (Fig. 9), and thus are predicted to be anchoring ligands to the site B Zn(II) (Fig. 8A). Consistent with this role, D118 (H118 in *Spn*; see Fig. S1), when substituted with Cys (D118C), forms a direct coordination bond to the metal. It is interesting to note in this context that in four streptococcal strains, *S. anginosus*, *S. intermedius*, *S. gordonii* and *S. sanguinis*, H67 is a Gln (Q) and H118 is a Tyr (Y) (Fig. S1). Although neither Gln or Tyr are common Zn ligands, neither is unprecedented, with Gln found in approximately 0.1% of all functional Zn(II)-binding sites in crystallographically characterized proteins (Laitaoja *et al.*, 2013; Chan *et al.*, 2015). However, the double H67Q/H118Y substitution may result in loss of site B in these streptococci SczAs altogether, further evidence for which is an additional H117N substitution in the *S. gordonii* SczA sequence (Fig. S1). These findings suggest the probability that only the A-site is strictly evolutionarily conserved and that different SczAs may function via distinct allosteric mechanisms.

The remaining candidate B-site ligands (Fig. 8A) differentially impact SczA function. The *sczA*-E114A strain shows a moderate growth phenotype in liquid culture and within the intramacrophage microenvironment. This may be consistent with the partial retention of a weak band at 560 nm in the Co(II) absorption spectra *in vitro* with purified SczA-E114A mutant

protein, suggesting that there may be a small degree of residual tetrahedral binding by this mutant. H117, on the other hand, appears to be crucial for tetrahedral Co(II) binding *in vitro*, but mutation results in no strong phenotype *in vivo*. Like H84 and H88, H114 and H117 likely contribute to chelate stability and mutating both H117 and H114 simultaneously may be necessary to observe a stronger Zn-resistance phenotype.

Interestingly, prior structural studies of other bacterial Zn(II)-sensing transcriptional regulators also reveal the presence of two distinct metal-binding sites that are required, albeit to variable degrees, for activation of DNA binding and transcriptional repression. The metal ions associated with these sites are typically coordinated by His or carboxylate residues, although in at least one case, cysteine is a ligand (Guerra *et al.*, 2011). Two regulatory metal sites are found in the zinc uptake repressors (Zur) from *Mycobacterium tuberculosis* (Lucarelli et al., 2007), *B. subtilis* (Ma *et al.*, 2011; Shin and Helmann, 2016) and *Streptomyces coelicolor* (Shin *et al.*, 2011), and in the adhesin competence regulator (AdcR) from *S. pneumoniae* (Guerra *et al.*, 2011) and *S. pyogenes* (Sanson *et al.*, 2015). In these systems, immediately adjacent residues in the primary structure make coordination bonds to two different Zn(II) ions. Although coordination by vicinal His or one of two Glu-His (E-H) sequences (in AdcR) are under-represented in catalytic and structural Zn(II) coordination sites in proteins, relative to more typical HxH and HxxxH motifs found in β-strands and α-helices, respectively (Vallee and Auld, 1990), such an arrangement is clearly not uncommon among Zn(II)-sensing metallosensors. The "second" or ancillary site has been shown in several of cases to fine-tune the transcriptional repression of specific genes leading to a hierarchy of repression or a "graded response" as bioavailable Zn(II) rises in the cell (Shin *et al.*, 2011; Shin and Helmann, 2016). The two metal sites in SczA,

however, are unlikely to facilitate a graded transcriptional response, since Zn(II) is an allosteric *activator* of transcription, and the only known regulatory target in cells is *czcD*.

Elucidation of the precise mode of Zn(II) coordination in sites A and B in SczA will require high resolution structural analyses beyond the scope of this study. As shown here, substitution of a subset of the predicted metal coordinating ligands results in a differential impact on SczA function. At first glance, the simultaneous coordination of H67 and H68 to distinct metals (A, B) (see Fig. 8A) might be expected to require local unwinding or partial distortion of the α4 helical geometry and thereby properly orient the site B ligands into a tetrahedral geometry around a Zn(II) ion, without concomitant disruption of Zn(II) binding to site A. Such a structural rearrangement may be necessary to drive the allosteric activation of SczA, via an impact on DNA binding or a protein-protein interaction. On the other hand, the E41-H42 and E107-H108 dipeptide pairs in AdcR, where the first and second residues of each forms coordination bonds to secondary site 2 and primary site 1 Zn(II) ions (Guerra *et al.*, 2011) respectively, occur without significant distortion of the α2 and α5 helices, respectively, from which they are derived.

Assignment of the high and low affinity Zn(II) binding sites in SczA (see Fig. 5) cannot be clearly defined by these data, and will require a site-specific NMR titration analyses (see Fig. S8). Although Co(II) fills site A first followed by site B, the order of occupancy is likely reversed for Zn(II), given the finding that Zn(II) displaces the B-site Co(II) prior to displacement of the A-site metal (Fig. 6B). This assignment is fully compatible with predictions from ligand field stabilization energies, as the relative affinities of high spin Co(II) toward a tetrahedral complex will be 10^3-10^5-fold lower than that for Zn(II), with this differential much smaller for pentacoordinate and octahedral sites (Guo and Giedroc, 1997; Guerrerio and Berg, 2004). Thus, we favor a model in which the tetrahedral B-site is the high affinity metal site and the higher

coordination number A-site serving as the lower affinity site in SczA (Fig. 8B). However, the structural integrity of both sites is clearly necessary for transcriptional activation and protection from zinc toxicity in infected macrophages, irrespective of the mechanism. Indeed, filling of the A-site alone, at least by a non-cognate metal Ni(II), does not appear to stabilize a "closed" DNA-binding competent form of the homodimer, as evidenced by the crystal structure (Fig. 2).

Our findings suggest that *S. pneumoniae*, and possibly other streptococci, are sensitive to fluctuations in intracellular free or rapidly exchangeable Zn(II). In fact, cellular growth rates and morphological changes are observed when WT *S. pneumoniae* D39 is grown in the presence of less than 200 μM extracellular Zn (Reyes-Caballero *et al.*, 2010; Martin and Giedroc, 2016; Martin *et al.*, 2017). These changes are even more pronounced in *czcD*-null efflux mutants. Note that the affinity of *S. pneumoniae* CzcD for Zn(II) is unknown, as is the degree of *czcD* transcriptional activation that is required to mitigate the effects of Zn toxicity in bacterial cells. However, Zn toxicity within infected macrophages is clearly implicated as a host-mediated strategy by which the innate immune response exploits the coordination chemistry of zinc to aid in the clearance of bacterial pathogens as they attempt to cause invasive disease. The growth phenotype and cellular morphology observed during Zn toxicity can be partially relieved by Mn supplementation but the extent to which metabolic processes remain affected by high levels of extracellular Zn or by perturbations in the bioavailable Mn/Zn ratio remains unclear.

In fact, our data provide further support that, at least for *S. pneumoniae*, Mn and Zn homeostasis are interconnected; we find that the Mn/Zn ratio can influence CzcD expression, likely via direct antagonization of SczA function by Mn (Fig. 10). Clearly, an intimate coupling of the A- and B-metal sites in SczAs may well facilitate sensitivity to cellular Zn/Mn ratios, analogous to that described previously for the Mn(II)-activated repressor PsaR (Lisher *et al.*,

2013). Here, Zn(II) binding to the regulatory sites on the PsaR homodimer under conditions of Zn(II) toxicity inhibits allosteric activation of DNA binding by Mn(II). One exciting possibility is that non-cognate Mn(II) binds to the A-site and adopts a non-native coordination structure, which fails to displace SczA from OP1. Under conditions where Mn is limiting and/or Zn is abundant, Zn will displace Mn from SczA site A, inducing a conformational change and/or distinct coordination structure, resulting in an increase in DNA affinity for OP2 thus driving operator switching by SczA (see Fig. 1). Future studies will focus on understanding how the Mn/Zn ratio affects the structure and the dynamics of the SczA homodimer, both off and on the DNA operator, and elucidation of the complex network of allosteric linkage of metal binding and transcriptional activation of CzcD expression by SczA.

Experimental procedures

Bacterial strain and plasmid construction

The strains used in the study were derived from *S. pneumoniae* D39 serotype 2 (IU1781) and are listed in Table S1. All mutants were constructed by gene deletion replacement and counter antibiotic selection using the *kan-rpsL*$^+$ cassette, Janus (Sung *et al.*, 2001). Briefly, the 0.8 to 1-kb region upstream and downstream of target genes were amplified from genomic DNA using inner primers containing flanking regions to the kanamycin-resistant Janus cassette (*kan-rpsL*$^+$). The two outside fragments generated were then joined together with the inner *kan-rpsL*$^+$ fragment. The final PCR product was transformed into competent *rpsL1* pneumococcal cells using standard techniques (Tsui *et al.*, 2010). Bacteria were grown on trypticase soy agar II plates containing 5% (v/v) defibrinated sheep blood (TSAII-BA; Becton Dickinson). Plates were incubated at 37°C in an atmosphere of 5% CO_2. TSAII-BA plates contained 250 μg/mL

kanamycin, 250 μg/mL streptomycin, or 0.3 μg/mL erythromycin (Sigma-aldrich) for antibiotic selection.

For construction of C-terminal single-FLAG-tagged SczA expressed from its native promoter, overlapping 1.5-kb fragments were generated by PCR using primers with the flanking FLAG-tag sequence 5'-GATTATAAAGATGATGATGATAAA-3' and IU1781 as genomic template. Fragments were then joined together with a P_c-*erm*^{R} resistance marker and transformed into competent IU10393 (*czcD*-FLAG) (Martin and Giedroc, 2016) cells for allelic replacement at the native *sczA* locus and selected for erythromycin resistance. Strains containing C-terminal triple-FLAG-tagged SczA of both *S. pneumoniae* and *S. agalactiae* were constructed similarly with a 10 amino acid linker (5'-ggttccgctggctccgctgctggttctggc-3') inserted before the triple FLAG tag (5'-gattataaagatgatgataaagattataaagatgatgataaagattataaagatgatgataaataa-3'; stop codon underlined) generating *sczA*-L-FLAG^3-P_c-*erm*^{R}.

Site-directed mutagenesis was used to generate amplicons containing chromosomal allelic substitution in *sczA*. Briefly, complementary primers were designed with the mutation of interest located in the center of the sequence. Overlapping fragments generated by PCR were joined together and transformed into competent IU10393 (*czcD*-FLAG) (Martin and Giedroc, 2016) cells and selected for erythromycin-resistance. All resulting strain constructs were confirmed by DNA sequencing through relevant portions of the genome.

All plasmids used in this study are listed in Table S1. Plasmid pSPN01 was constructed by amplifying the *sczA* ORF from *S. pneumoniae* D39 genomic DNA. The PCR product was digested with *Nde*I and *Bam*HI, ligated into pET3a behind a T7 promoter, transformed into *E. coli* DH5α, and selected for ampicillin-resistance (100 μg/mL) on LB agar. Plasmid pSAG01

was constructed similarly to pSPN01 after obtaining *S. agalactiae sczA* (gene locus SAG0431) using total gene synthesis from DNA oligos that were codon optimized (Hoover and Lubkowski, 2002). Site-directed mutagenesis was used to generate amino acid substitutions in SczA on plasmid pSAG01. All resulting plasmid constructs were DNA sequence verified.

Expression and purification of SczA

Plasmid DNA was transformed into *Escherichia coli* Rosetta (DE3) pLysS (Novagen) the day before planned expression of SczA and selected on LB agar plates containing 100 μg/mL ampicillin and 24 μg/mL chloramphenicol. The bacteria were scraped from the plate and used to inoculate 15 mL LB broth containing only ampicillin. At approximately 0.6 OD_{600}, cells were diluted 1/100 into fresh LB broth containing only ampicillin and grown aerobically at 37°C. At approximately 0.6 OD_{600}, 1 mM isopropyl β-D-1-thiogalactopyranoside was added to induce SczA protein synthesis. One-liter of cells were harvested after 18 h at 18°C by centrifugation. Cells were suspended in lysis buffer (25 mM Tris-HCl, pH 8.0, 1 M NaCl, 2 mM EDTA, 1 mM DTT) and disrupted by sonication on ice (1/2 in. probe at 30 % power for 300 cycles, 1 s pulse on and 5 s pulse off). Cell debris was removed by centrifugation. SczA proteins were precipitated from cell lysate by 70% saturation with ammonium sulfate, then suspended and dialyzed overnight at 4°C against 2x1 L of buffer A (25 mM Tris-HCl, pH 8.0, 200 mM NaCl, 7 mM β-mercaptoethanol) or buffer QA (25 mM Tris-HCl, pH 8.0, 75 mM NaCl, 1 mM DTT) for initial purification step on Ni(II)-NTA affinity or sepharose Q column, respectively. Wild-type SczA, site B mutants, and N-terminal mutants (R6A and K10A) were flowed over a HIStrap HP Ni(II)-NTA column (GE Life Sciences). Bound proteins were eluted in buffer A with a gradient of 0-200 mM imidazole, dialyzed against overnight at 4°C overnight against 1 L buffer QA, and

then further purified using a mono Q column (GE Life Sciences). Fractions containing SczA protein were pooled, concentrated, and separated further on a HiLoad 16/600 Superdex 75 size-exclusion column (GE Life Sciences) equilibrated with buffer G (25 mM Tris-HCl, pH8.0, 500 mM NaCl, 2 mM EDTA, 2 mM dithiothritol (DTT)). Fractions containing SczA protein were pooled and concentrated. Divalent metal cations were removed by dialyzing protein against 25 mM Hepes, pH 7.0, 400 mM NaCl, 2 mM tris(2-carboxyethyl)phosphine (TCEP) buffer containing 10 g/L Chelex-100 resin. Site A metal-binding mutant SczA variants were purified using sepharose Q, then gel filtration before final dialysis to remove divalent metal cations; Ni(II)-NTA was not used. Purity of protein was visualized by 15 % polyacrylamide gel electrophoresis. Mass spectrometry (ESI-MS and MALDI-TOF) was performed to confirm the identity of the final protein. Protein concentrations were calculated using predicted extinction coefficient for each SczA construct at 280 nm (Protparam) (Gasteiger *et al.*, 2005).

Metal-binding stoichiometry and affinity determinations.

For Zn(II) metal-binding experiments, purified apo-SczA protein stocks were incubated with 5 mM EDTA, pH 8.0 at room temperature and then extensively dialyzed into 25 mM Hepes, pH 8.0, 200 mM NaCl, 1 mM TCEP or 25 mM MES, pH 6.0, 200 mM NaCl, 1 mM TCEP to remove EDTA. All apo-protein stocks were confirmed as metal-free using inductively-coupled plasma-mass spectrometry (ICP-MS). Apo-protein (1 μM) was diluted into metal-free buffer. A fixed concentration (1 μM) of metal-free mag-fura-2 (mf2) was added to the solution to reach a final volume of 2 mL. Data was collected using an ISS PC1 spectrofluorometer with 1.0 mm beam and emission slits in continuous excitation mode, measuring 505 nm emission as a

function of the excitation wavelength, every two min after each *i*th addition of Zn(II) at 25°C. The Zn(II) binding affinity for mf2 at pH 8.0 measured 8.6 x 10^6 M^{-1}.

For Mn(II) metal-binding experiments, purified apo-SczA protein stocks were incubated with 5 mM EDTA, pH 8.0 at room temperature, then extensively dialyzed into 10 mM Hepes, pH 7.2, 400 mM NaCl to remove EDTA, and confirmed metal-free by ICP-MS. Apo-protein was diluted into metal-free buffer. A fixed concentration of metal-free mf2 was added to the solution to reach a final volume of 1 mL. Metal stock of Mn(II) was titrated into the protein-competitor solution and the absorbance at 360 nm and 325 nm were monitored which report on the λmax for the metal-free and metal-bound states of the mf2 (Lisher *et al.*, 2013), respectively, were taken after 2 min incubation using a Hewlett-Packard model 8452A spectrophotometer at room temperature. All metal-binding data were fitted to an appropriate one-step competition binding model using Dynafit (Kuzmic, 1996).

Cobalt titration assay

Apo-SczA protein was exchanged into metal-free 10 mM Hepes, pH 7.2, 400 mM NaCl buffer, at concentrations ranging from 0.25-0.55 mM. Metal stock of Co(II) was titrated into the protein solution and absorbance spectra were recorded between 250 nm and 800 nm after 1 min incubation at room temperature using a Hewlett-Packard model 8452A spectrophotometer.

Nuclear magnetic resonance (NMR) spectroscopy

Isotope-labeled SczA for NMR experiments was prepared by overexpression in *E. coli* (Rosetta DE3-pLysS; Novagen) in M9 minimal media containing $^{15}NH_4Cl$ and ^{2}H,^{13}C-labeled glucose and purified as described above. NMR samples contained 0.25-0.3 mM U-^{2}H,^{13}C,^{15}N

SczA, 25 mM MES, 300 mM NaCl, 1 mM TCEP, 10% D_2O at pH 6.5, and were supplemented with equimolar $MnCl_2$ when indicated. Chemical shifts were referenced to 2,2-dimethyl-2-silapentaene-5-sulfonic acid (DSS; Sigma). NMR spectra were acquired at 30°C with a Varian DDR 800 MHz or 600 MHz spectrometer equipped with a cryogenic probe at the Indiana University METACyt Biomolecular NMR Laboratory. Spectra were processed using NMRPipe (Delaglio *et al.*, 1995). 3-dimensional spectra were acquired using nonuniform sampling and reconstructed using hmsIST (Hyberts *et al.*, 2012) and analyzed using SPARKY (Goddard and Kneller) or CARA (Keller, 2004). Sequential resonance assignments for the apo form were obtained using a 2D $^{1}H,^{15}N$ TROSY (Pervushin *et al.*, 1997) spectrum and TROSY versions of the following triple resonance spectra: HNCA, HN(CO)CA, HNCO, HN(CA)CO, HN(CA)CB, HN(COCA)CB (Salzmann *et al.*, 1999). The ^{15}N-$\{^{1}H\}$ heteronuclear NOE was also recorded using TROSY (Renner *et al.*, 2002), and secondary structure predictions based on chemical shifts were made using TALOS+ (Shen *et al.*, 2009). Backbone resonance assignments have been deposited in the BioMagResBank (BMRB) under accession number 26658.

Growth conditions for *S. pneumoniae*

Brain-heart infusion (BHI; Becton, Dickinson and Company) medium was of standard composition and prepared with double distilled water. Standard BHI broth contained ≈18 μM Zn in final preparation. For growth experiments, bacteria were inoculated into BHI broth from frozen culture stocks, then serially diluted and grown overnight at 37°C in an atmosphere of 5% CO_2. Overnight exponentially growing cultures were diluted to an optical density at 620 nm (OD_{620}) of 0.006 into pre-warmed BHI containing increasing concentrations of $ZnSO_4$ (Alfa

Aesar). All aerobic cell growth experiments were monitored over time at 37°C in an atmosphere of 5% CO_2.

Western blot analysis of CzcD and SczA protein

Protein expression was determined from strains harboring chromosomal fusions of single-FLAG-tagged CzcD and triple- or single-FLAG-tagged SczA grown to approximately 0.15 OD_{620} in BHI and treated with 200 μM $ZnSO_4$ for 40 min. Cells were centrifuged, washed with ice-cold phosphate buffered saline (PBS), pH 7.4, resuspended in 1/35 the original culture volume with PBS, pH 7.4 containing 1% sodium dodecyl sulfate, 0.1% triton X-100 and 0.5 mg DNase, and lysed at 37°C for 30 min. Cell lysates were diluted into 2x Laemmli sample buffer (BioRad) containing β-mercaptoethanol and heated at 95°C for 10 min. Proteins (15 μg) were separated by SDS-PAGE and transferred to a nitrocellulose membrane. Membranes were blocked with 5% membrane block agent (ECL; GE Healthcare) in PBS, pH 7.4 containing 0.1% Tween 20 (PBST) and probed with anti-FLAG rabbit polyclonal antibody (Sigma-aldrich) in PBST. Proteins were detected using anti-rabbit antibody linked to horse radish peroxidase and ECL western blotting reagent. Western blots were imaged using an image vision system.

For experiments examining the effect of bioavailable Mn:Zn ratio on SczA function. Exponentially growing WT and *mntE*-null strains harboring the CzcD-FLAG allele were diluted to 0.006 OD_{620} into pre-warmed BHI with or without 200 μM $MnCl_2$ (Sigma-Aldrich). After approximately 3.5 h of growth, increasing concentrations of $ZnSO_4$ was added to cultures. Cells were harvested after 1 h incubation at 37°C with 5% CO_2 and prepared for western blot analysis as described above. The statistical differences between non-stressed and Mn-stressed samples were examined using student *t*-test (unpaired test with Welch's correction).

Inductively coupled plasma-mass spectrometry (ICP-MS) for measurement of total cell-associated zinc

The total cell-associated Zn was quantified from 5 mL cultures that had been grown in BHI with or without 0.2 mM $ZnSO_4$ for 4 h. Cells were centrifuged, washed once with ice-cold PBS, pH 7.4 containing 2 mM nitrilotriacetic acid (NTA; Sigma-Aldrich, St. Louis, MO), washed twice with ice-cold metal-free PBS (10 g/L Chelex-100 resin was used to remove metals), pH 7.4, and dried for 2 h using a centrifuge evaporator. Dried cells were solubilized in 400 µL 30% (v/v) HNO_3 (Sigma-Aldrich, St. Louis, MO) and lysed by incubating at 95°C for 10 min shaking at 500 rpm. ICP-MS samples were prepared by diluting 300 µL of lysed cells into 2.7 ml 2.5% (v/v) HNO_3. Metal concentrations were calculated from the standard curve using 1 to 30 ppb metal stock solutions and normalized to total protein determined using DC™ protein assay (BioRad).

***S. pneumoniae* survival in macrophages**

THP-1 cells (ATCC TIB-202) were grown under atmospheric control (95% air and 5% CO_2) at 37 °C in complete RPMI medium [RPMI with phenol red (Thermo-Fisher Scientific), supplemented with 10% fetal bovine serum, 10 mM HEPES, 30 µg/mL penicillin and 50 µg/mL streptomycin]. Cell culture flasks (25 cm^2; BD Falcon) were seeded with 3.5×10^6 THP-1 cells and differentiated by adding 100 ng/mL phorbol 12-myristate 13-acetate (PMA; Merck) and incubated for three days. Attached differentiated THP-1 cells (macrophages) were washed in complete RPMI and incubated with complete RPMI without added PMA to allow resting for a minimum of 2 days. One hour before challenge with *S. pneumoniae*, macrophages were

detached using 1 mL StemPro Accutase (Thermo Fisher Scientific), washed in Hank's Balanced Salt Solution (HBSS; Thermo Fisher Scientific) and diluted to 1.1×10^5 cells/mL in HBSS. WT *S. pneumoniae* D39 and the *sczA* mutant variants were grown overnight on blood agar plates at 37°C in an atmosphere of 5% CO_2 and subsequently inoculated into C+Y media (Begg *et al.*, 2015) to an optical density at 600 nm (OD_{600}) of 0.05. At 0.3 OD_{600}, cells were washed, resuspended in HBSS, and colony forming unit (CFU) counts determined by plating on blood agar. The macrophages and *S. pneumoniae* cells were co-incubated at a ratio of 1:10 for 90 min, then washed and incubated with 200 µg/mL gentamycin and 10 µg/mL penicillin for 30 min to kill extracellular bacteria. The macrophages were then washed in HBSS without antibiotic and incubated for an additional 60 min prior to analysis of intracellular bacteria by lysing the macrophages with 0.0625% Triton-X-100. The lysate was then plated onto blood agar. The CFUs were enumerated, corrected for input, and normalized to values obtained for the WT strain. The data represent the mean of five biological replicates (±SEM). The statistical differences between the mutant variants and the control (WT) were examined using a one-way ANOVA with Dunnett's post-test.

Acknowledgements

We thank Dr. John P. Lisher for help with ICP-MS analysis, Dr. Hongwei Wu for help in acquiring NMR spectra, and Adriana Giuliani and Katherine Geiger for help in early cloning of and *in vitro* mutagenesis experiments with *S. pneumoniae* SczA. This work was supported by NIH grants GM042569 and GM118157 (to D.P.G.), GM113172 and GM114315 (to M.E.W), and Australian Research Council Discovery Project Grant DP150101856 (to C.A.M). The NMR instrumentation in the METACyt Biomolecular NMR Laboratory at Indiana University was generously supported by a grant from the Lilly Endowment.

References

Andreini, C., Banci, L., Bertini, I. and Rosato, A. (2006) Zinc through the three domains of life. *J Proteome Res* **5**: 3173-3178.

Anton, A., Grosse, C., Reissmann, J., Pribyl, T. and Nies, D.H. (1999) CzcD is a heavy metal ion transporter involved in regulation of heavy metal resistance in *Ralstonia sp*. strain CH34. *J Bacteriol* **181**: 6876-6881.

Begg, S.L., Eijkelkamp, B.A., Luo, Z., Counago, R.M., Morey, J.R., Maher, M.J., Ong, C.L., McEwan, A.G., Kobe, B., O'Mara, M.L., Paton, J.C. and McDevitt, C.A. (2015) Dysregulation of transition metal ion homeostasis is the molecular basis for cadmium toxicity in *Streptococcus pneumoniae*. *Nat Commun* **6**: 6418.

Bijlsma, J.J., Burghout, P., Kloosterman, T.G., Bootsma, H.J., de Jong, A., Hermans, P.W. and Kuipers, O.P. (2007) Development of genomic array footprinting for identification of conditionally essential genes in *Streptococcus pneumoniae*. *App Environ Microbiol* **73**: 1514-1524.

Bonaventura, P., Benedetti, G., Albarede, F. and Miossec, P. (2015) Zinc and its role in immunity and inflammation. *Autoimmun Rev* **14**: 277-285.

Botella, H., Peyron, P., Levillain, F., Poincloux, R., Poquet, Y., Brandli, I., Wang, C., Tailleux, L., Tilleul, S., Charriere, G.M., Waddell, S.J., Foti, M., Lugo-Villarino, G., Gao, Q., Maridonneau-Parini, I., Butcher, P.D., Castagnoli, P.R., Gicquel, B., de Chastellier, C. and Neyrolles, O. (2011) Mycobacterial p(1)-type ATPases mediate resistance to zinc poisoning in human macrophages. *Cell Host Microbe* **10**: 248-259.

Capdevila, D.A., Wang, J. and Giedroc, D.P. (2016) Bacterial strategies to maintain zinc metallostasis at the host-pathogen interface. *J Biol Chem* **291**: 20858-20868.

Chan, A.C., Blair, K.M., Liu, Y., Frirdich, E., Gaynor, E.C., Tanner, M.E., Salama, N.R. and Murphy, M.E. (2015) Helical shape of *Helicobacter pylori* requires an atypical glutamine as a zinc ligand in the carboxypeptidase Csd4. *J Biol Chem* **290**: 3622-3638.

Counago, R.M., Ween, M.P., Begg, S.L., Bajaj, M., Zuegg, J., O'Mara, M.L., Cooper, M.A., McEwan, A.G., Paton, J.C., Kobe, B. and McDevitt, C.A. (2014) Imperfect coordination chemistry facilitates metal ion release in the Psa permease. *Nat Chem Biol* **10**: 35-41.

Cuthbertson, L. and Nodwell, J.R. (2013) The TetR family of regulators. *Microbiol Mol Biol Rev* **77**: 440-475.

Delaglio, F., Grzesiek, S., Vuister, G.W., Zhu, G., Pfeifer, J. and Bax, A. (1995) NMRPipe: a multidimensional spectral processing system based on UNIX pipes. *J Biomol NMR* **6**: 277-293.

Djoko, K.Y., Ong, C.L., Walker, M.J. and McEwan, A.G. (2015) The role of copper and zinc toxicity in innate immune defense against bacterial pathogens. *J Biol Chem* **290**: 18954-18961.

Eijkelkamp, B.A., Morey, J.R., Ween, M.P., Ong, C.L., McEwan, A.G., Paton, J.C. and McDevitt, C.A. (2014) Extracellular zinc competitively inhibits manganese uptake and compromises oxidative stress management in *Streptococcus pneumoniae*. *PloS One* **9**: e89427.

Gasteiger, E., Hoogland, C., Gattiker, A., Duvaud, S., Wilkins, M.R., Appel, R.D. and Bairoch, A. (2005) Protein identification and analysis tools on the ExPASy server. In: The proteomics protocols handbook. Walker, J.M. (ed). Humana Press, pp. 571-607.

Goddard, T.D. and Kneller, D.G. Sparky 3. University of California, San Francisco.

Guerra, A.J., Dann, C.E. and Giedroc, D.P. (2011) Crystal structure of the zinc-dependent MarR family transcriptional regulator AdcR in the Zn(II)-bound state. *J Am Chem Soc* **133**: 19614-19617.

Guerrerio, A.L. and Berg, J.M. (2004) Metal ion affinities of the zinc finger domains of the metal responsive element-binding transcription factor-1 (MTF1). *Biochemistry* **43**: 5437-5444.

Guo, J. and Giedroc, D.P. (1997) Zinc site redesign in T4 gene 32 protein: structure and stability of cobalt(II) complexes formed by wild-type and metal ligand substitution mutants. *Biochemistry* **36**: 730-742.

Hantke, K. (2001) Bacterial zinc transporters and regulators. *Biometals* **14**: 239-249.

Honsa, E.S., Johnson, M.D. and Rosch, J.W. (2013) The roles of transition metals in the physiology and pathogenesis of *Streptococcus pneumoniae*. *Front Cell Infect Microbiol* **3**: 92.

Hoover, D.M. and Lubkowski, J. (2002) DNAWorks: an automated method for designing oligonucleotides for PCR-based gene synthesis. *Nucleic Acids Res* **30**: e43.

Hyberts, S.G., Milbradt, A.G., Wagner, A.B., Arthanari, H. and Wagner, G. (2012) Application of iterative soft thresholding for fast reconstruction of NMR data non-uniformly sampled with multidimensional poisson gap scheduling. *J Biomol NMR* **52**: 315-327.

Imlay, J.A. (2014) The mismetallation of enzymes during oxidative stress. *J Biol Chem* **289**: 28121-28128.

Jacobsen, F.E., Kazmierczak, K.M., Lisher, J.P., Winkler, M.E. and Giedroc, D.P. (2011) Interplay between manganese and zinc homeostasis in the human pathogen *Streptococcus pneumoniae*. *Metallomics* **3**: 38-41.

Keller, R.L.J. (2004) The computer aided resonance assignment tutorial. Goldau: Cantina Verlag. pp. 1-81.

Kloosterman, T.G., van der Kooi-Pol, M.M., Bijlsma, J.J. and Kuipers, O.P. (2007) The novel transcriptional regulator SczA mediates protection against Zn^{2+} stress by activation of the Zn^{2+}-resistance gene *czcD* in *Streptococcus pneumoniae*. *Mol Microbiol* **65**: 1049-1063.

Kloosterman, T.G., Witwicki, R.M., van der Kooi-Pol, M.M., Bijlsma, J.J. and Kuipers, O.P. (2008) Opposite effects of Mn^{2+} and Zn^{2+} on PsaR-mediated expression of the virulence genes *pcpA, prtA*, and *psaBCA* of *Streptococcus pneumoniae*. *J Bacteriol* **190**: 5382-5393.

Kuzmic, P. (1996) Program DYNAFIT for the analysis of enzyme kinetic data: application to HIV proteinase. *Anal Biochem* **237**: 260-273.

Laitaoja, M., Valjakka, J. and Janis, J. (2013) Zinc coordination spheres in protein structures. *Inorg Chem* **52**: 10983-10991.

Larkin, M.A., Blackshields, G., Brown, N.P., Chenna, R., McGettigan, P.A., McWilliam, H., Valentin, F., Wallace, I.M., Wilm, A., Lopez, R., Thompson, J.D., Gibson, T.J. and Higgins, D.G. (2007) Clustal W and Clustal X version 2.0. *Bioinformatics* **23**: 2947-2948.

Le, T.B., Schumacher, M.A., Lawson, D.M., Brennan, R.G. and Buttner, M.J. (2011) The crystal structure of the TetR family transcriptional repressor SimR bound to DNA and the role of a flexible N-terminal extension in minor groove binding. *Nucleic Acids Res* **39**: 9433-9447.

Lisher, J.P., Higgins, K.A., Maroney, M.J. and Giedroc, D.P. (2013) Physical characterization of the manganese-sensing pneumococcal surface antigen repressor from *Streptococcus pneumoniae*. *Biochemistry* **52**: 7689-7701.

Lucarelli, D., Russo, S., Garman, E., Milano, A., Meyer-Klaucke, W. and Pohl, E. (2007) Crystal structure and function of the zinc uptake regulator FurB from *Mycobacterium tuberculosis*. *J Biol Chem* **282**: 9914-9922.

Ma, Z., Gabriel, S.E. and Helmann, J.D. (2011) Sequential binding and sensing of Zn(II) by *Bacillus subtilis* Zur. *Nucleic Acids Res* **39**: 9130-9138.

Martin, J.E. and Giedroc, D.P. (2016) Functional determinants of metal ion transport and selectivity in paralogous cation diffusion facilitator transporters CzcD and MntE in *Streptococcus pneumoniae*. *J Bacteriol* **198**: 1066-1076.

Martin, J.E., Lisher, J.P., Winkler, M.E. and Giedroc, D.P. (2017) Perturbation of manganese metabolism disrupts cell division in *Streptococcus pneumoniae*. *Mol Microbiol*: in the press.

McCall, K.A., Huang, C. and Fierke, C.A. (2000) Function and mechanism of zinc metalloenzymes. *J Nutr* **130**: 1437S-1446S.

McDevitt, C.A., Ogunniyi, A.D., Valkov, E., Lawrence, M.C., Kobe, B., McEwan, A.G. and Paton, J.C. (2011) A molecular mechanism for bacterial susceptibility to zinc. *PLoS pathogens* **7**: e1002357.

Milanino, R., Marrella, M., Gasperini, R., Pasqualicchio, M. and Velo, G. (1993) Copper and zinc body levels in inflammation: an overview of the data obtained from animal and human studies. *Agents Actions* **39**: 195-209.

Nairn, B.L., Lonergan, Z.R., Wang, J., Braymer, J.J., Zhang, Y., Calcutt, M.W., Lisher, J.P., Gilston, B.A., Chazin, W.J., de Crecy-Lagard, V., Giedroc, D.P. and Skaar, E.P. (2016) The response of *Acinetobacter baumannii* to zinc starvation. *Cell Host Microbe* **19**: 826-836.

Ogunniyi, A.D., Mahdi, L.K., Jennings, M.P., McEwan, A.G., McDevitt, C.A., Van der Hoek, M.B., Bagley, C.J., Hoffmann, P., Gould, K.A. and Paton, J.C. (2010) Central role of manganese in regulation of stress responses, physiology, and metabolism in *Streptococcus pneumoniae*. *J Bacteriol* **192**: 4489-4497.

Ong, C.L., Gillen, C.M., Barnett, T.C., Walker, M.J. and McEwan, A.G. (2014) An antimicrobial role for zinc in innate immune defense against group A streptococcus. *J Infect Dis* **209**: 1500-1508.

Ong, C.L., Walker, M.J. and McEwan, A.G. (2015) Zinc disrupts central carbon metabolism and capsule biosynthesis in *Streptococcus pyogenes*. *Sci Rep* **5**: 10799.

Orth, P., Schnappinger, D., Hillen, W., Saenger, W. and Hinrichs, W. (2000) Structural basis of gene regulation by the tetracycline inducible Tet repressor-operator system. *Nat Struct Biol* **7**: 215-219.

Pennella, M.A., Arunkumar, A.I. and Giedroc, D.P. (2006) Individual metal ligands play distinct functional roles in the zinc sensor *Staphylococcus aureus* CzrA. *J Mol Biol* **356**: 1124-1136.

Pennella, M.A., Shokes, J.E., Cosper, N.J., Scott, R.A. and Giedroc, D.P. (2003) Structural elements of metal selectivity in metal sensor proteins. *Proc Natl Acad Sci USA*. **100**: 3713-3718.

Pervushin, K., Riek, R., Wider, G. and Wuthrich, K. (1997) Attenuated T2 relaxation by mutual cancellation of dipole-dipole coupling and chemical shift anisotropy indicates an avenue to NMR structures of very large biological macromolecules in solution. *Proc Natl Acad Sci USA* **94**: 12366-12371.

Ramos-Montanez, S., Tsui, H.C., Wayne, K.J., Morris, J.L., Peters, L.E., Zhang, F., Kazmierczak, K.M., Sham, L.T. and Winkler, M.E. (2008) Polymorphism and regulation of the *spxB* (pyruvate oxidase) virulence factor gene by a CBS-HotDog domain protein (SpxR) in serotype 2 *Streptococcus pneumoniae*. *Mol Microbiol* **67**: 729-746.

Renner, C., Schleicher, M., Moroder, L. and Holak, T.A. (2002) Practical aspects of the 2D 15N-[1h]-NOE experiment. *J Biomol NMR* **23**: 23-33.

Reyes-Caballero, H., Guerra, A.J., Jacobsen, F.E., Kazmierczak, K.M., Cowart, D., Koppolu, U.M., Scott, R.A., Winkler, M.E. and Giedroc, D.P. (2010) The metalloregulatory zinc site in *Streptococcus pneumoniae* AdcR, a zinc-activated MarR family repressor. *J Mol Biol* **403**: 197-216.

Robert, X. and Gouet, P. (2014) Deciphering key features in protein structures with the new ENDscript server. *Nucleic Acids Res* **42**: W320-324.

Salzmann, M., Wider, G., Pervushin, K. and Wuthrich, K. (1999) Improved sensitivity and coherence selection for [15N,1H]-TROSY elements in triple resonance experiments. *J Biomol NMR* **15**: 181-184.

Sanson, M., Makthal, N., Flores, A.R., Olsen, R.J., Musser, J.M. and Kumaraswami, M. (2015) Adhesin competence repressor (AdcR) from *Streptococcus pyogenes* controls adaptive responses to zinc limitation and contributes to virulence. *Nucleic Acids Res* **43**: 418-432.

Schumacher, M.A., Miller, M.C., Grkovic, S., Brown, M.H., Skurray, R.A. and Brennan, R.G. (2002) Structural basis for cooperative DNA binding by two dimers of the multidrug-binding protein QacR. *Embo J* **21**: 1210-1218.

Shen, Y., Delaglio, F., Cornilescu, G. and Bax, A. (2009) TALOS+: a hybrid method for predicting protein backbone torsion angles from NMR chemical shifts. *J Biomol NMR* **44**: 213-223.

Shin, J.H. and Helmann, J.D. (2016) Molecular logic of the Zur-regulated zinc deprivation response in *Bacillus subtilis*. *Nat Commun* **7**: 1-9.

Shin, J.H., Jung, H.J., An, Y.J., Cho, Y.-B., Cha, S.-S. and Roe, J.-H. (2011) Graded expression of zinc-responsive genes through two regulatory zinc-binding sites in Zur. *Proc Natl Acad Sci USA* **108**: 5045-5050.

Sung, C.K., Li, H., Claverys, J.P. and Morrison, D.A. (2001) An *rpsL* cassette, Janus, for gene replacement through negative selection in *Streptococcus pneumoniae*. *Appl Environ Microbiol* **67**: 5190-5196.

Tsui, H.C., Mukherjee, D., Ray, V.A., Sham, L.T., Feig, A.L. and Winkler, M.E. (2010) Identification and characterization of noncoding small RNAs in *Streptococcus pneumoniae* serotype 2 strain D39. *J Bacteriol* **192**: 264-279.

Vallee, B.L. and Auld, D.S. (1990) Active-site zinc ligands and activated H2O of zinc enzymes. *Proc Natl Acad Sci USA* **87**: 220-224.

Zalewski, P.D., Truong-Tran, A.Q., Grosser, D., Jayaram, L., Murgia, C. and Ruffin, R.E. (2005) Zinc metabolism in airway epithelium and airway inflammation: basic mechanisms and clinical targets. A review. *Pharmacol Ther* **105**: 127-149.

Main Figures

Figure 1. Schematic of the Zn-dependent mechanism of *czcD* transcription by SczA. (**A**) The *sczA-czcD* region in *S. pneumoniae* D39 serotype 2 highlighting the positions of the two previously characterized operators (OP1 and OP2) (Kloosterman *et al.*, 2007) and transcription start sites for the *sczA* and *czcD* genes. (**B**) When Zn is limiting, SczA binds to the *czcD* promoter blocking *czcD* transcription. However, when Zn is in excess, SczA binds upstream to OP1 inducing *czcD* expression, thereby increasing Zn efflux. Zn ions are represented by the *green* spheres.

Figure 2. Ribbon representation of the *Streptococcus agalactiae* SczA (SAG0431; PDB 3KKC) (*left*) highlighting the metal-binding A- and predicted B-sites within each protomer (*right*). Residue numbers correspond to *S. pneumoniae* SczA (which is consistently +1 relative to *S. agalactiae*; see Fig. 3). The residue marked H118 is an Asp (D117; designated here as D118) in the *Sag* SczA structure (see Figs. S1, Fig. 3). Color coding is as follows: N-terminal DNA binding domain, *magenta*; C-terminal regulatory domain, *blue*; Ni(II) ion, *green*.

Figure 3. Multiple sequence alignment of *Streptococcus agalactiae and Streptococcus pneumoniae* SczAs derived from a more extensive alignment (Figure S1). Ni(II)-binding residues in site A are designated by *green* spheres. *S. pneumoniae* SczA candidate metal-binding residues targeted in this study as site B are designated by *blue* or *white* spheres and DNA-binding residues by *yellow* spheres. Secondary structural elements of *S. agalactiae* SczA are shown as α-helices (coils; α1- α9) and residue numbering across the top refers to the *S. pneumoniae* SczA

sequence. *S. agalactiae* SczA and *S. pneumoniae* SczA exhibit 48% sequence identity. The alignment was generated using ClustalW (Larkin *et al.*, 2007), and the figure was prepared using ESPript (Robert and Gouet, 2014).

Figure 4. SczA is an important Zn-resistance determinant. Exponentially growing *S. pneumoniae* cells were diluted into pre-warmed BHI broth with 0 (*black*) or 300 μM Zn (*grey*) at *t*=0 and allowed to proliferate. Cell density after 6 h growth, post-inoculation is shown. Full growth curves are shown in Figure S2. Complementation of the *sczA*-null (Δ*sczA*) mutation by *S. pneumoniae* (spn) and *S. agalactiae* (sag) *sczA*-FLAG is shown. The mean of at least three independent cultures ± SEM is shown.

Figure 5. SczA binds two metal ions per protomer. Representative Zn(II) binding isotherms obtained from titrating Zn(II) into a solution of WT apo-SczA (1 μM) from *S. pneumoniae* (**A, B**) or *S. agalactiae* (**C**) with competitor mf2 (1 μM) at pH 8.0 (**A, C**) or pH 6.0 (**B**). *Open* symbols represent the 505 nm emission resulting from 324 nm excitation; *filled* symbols, 366 nm excitation; *red* lines represent data fit; *black* lines represent simulated curves of one order of magnitude less (*solid*) or more (*dashed*) for K_{Zn1} (see log *K* values in the main text).

Figure 6. Two distinct metal binding sites are observed in SczA spectroscopically. Co(II) titrations into *S. agalactiae* WT apo-SczA (**A**) and mutant variant apo-SczAs (**C-F**) monitored by UV-Vis electronic spectroscopy are plotted as protomer molar extinction coefficient (ε). (**B**) Plot of ε590 vs. protomer molar equivalence of Co(II) added to WT *S. agalactiae* SczA (*left*) followed by the addition of Zn(II) (*right*). These data collectively reveal a stoichiometry of two

Co(II) per protomer or four per dimer for SczA, with one site consistent with an octahedral coordination geometry and one site with a tetrahedral coordination geometry (see panel B).

Figure 7. Site specific mutations in DNA-binding helix 1, and candidate metal-binding clusters A and B residues of SczA increase Zn sensitivity. Exponentially growing cells were diluted into pre-warmed BHI broth with 0 (*black*) or 200 μM Zn (*grey*) at *t*=0 and allowed to proliferate. (**A**) Cell density after 6-h growth, post-inoculation. Full growth curves are shown in Figure S2. (**B**) Total cell-associated Zn measured by ICP-MS. Pneumococci lacking *czcD* accumulate ≥2-fold more Zn than WT strains during Zn stress as previously shown (Jacobsen *et al*., 2011; Martin and Giedroc, 2016). The mean of at least three independent cultures ± SEM is shown with statistical significance compared to WT strain. *, *p*-value≤0.05; **, *p*-value≤0.01; and ***, *p*-value≤0.001.

Figure 8. Candidate Zn(II) coordination complexes characteristic of metal-binding sites A and B in SczA. (**A**) Summary of spatial organization of metal binding sites on opposite sides of the α4 helix (see Fig. 2) based on Co(II) absorption spectra and functional data of WT and mutant *S. agalactiae* SczA proteins (see Figs. 6 and 7). Note that the precise Zn(II) coordination geometries shown are inferred from the Co(II) absorption spectra, and cannot be unambiguously defined by these data alone. ?, unknown. (**B**) Cartoon summary model of the relative activation of SczA by various metal cations tested in this study. The distorted tetrahedral B-site is the high affinity metal-binding site, while the A-site is likely octahedral, serving as the lower affinity site in SczA. Activation of *czcD* transcription by SczA requires filling of both sites A and B. Elevated Mn(II) levels can inhibit activation of SczA by Zn (see Fig. 10).

Figure 9. Intracellular survival of wild-type and SczA mutant variant *S. pneumoniae* strains in infected human macrophages. The data shown represent the mean of five biological replicates ±SEM. Significant differences to WT strain are shown. *, *p*-value≤0.05; **, *p*-value≤0.005; ***, *p*-value≤0.001; and ****, *p*-value≤0.0005.

Figure 10. The bioavailable Mn/Zn ratio influences CzcD expression. Exponentially growing WT (**A**) and *mntE*-null (**B**) strains were diluted into pre-warmed BHI broth with 0 (*black*) or 200 μM (*grey*) Mn at *t*=0 and allowed to grow for 3 h prior to adding Zn. Cells were harvested after 1 h and CzcD protein levels were detected by western blot (see Figure S6 for representative blots). The data shown represent the mean of three independent cultures that are normalized to non-stressed strains ± SEM. Significant differences to non-stressed strains are shown. *, *p*-value ≤0.10; ***, *p*-value ≤0.005; and ns, not significant. (**C**) TROSY spectra were recorded before and after addition of equimolar $MnCl_2$ to an NMR sample of apo-SczA. The change in peak height upon addition is shown for each residue. Unassigned residues, including prolines, are shaded grey. A threshold of 0.05 is shown as a dashed line. Error bars shown are propagated from S/N of each recorded spectrum. (**D**) The Mn(II)-induced paramagnetic relaxation enhancement data shown in panel C are plotted on the SczA crystal structure (PDB 3KKC), with residues impacted beyond the 0.05 cutoff colored *light grey*, and less affected residues colored *blue*. Unassigned residues, including prolines, are colored *dark grey*. Paramagnetic relaxation enhancement by the Mn(II) dramatically reduces signal intensities for nearby residues; as a result, many crosspeaks are missing or severely broadened in the presence

of Mn(II). Notably, residues in the metal-binding helices are most affected, while residues in the dimerization helices and the DNA-binding domain are less affected.

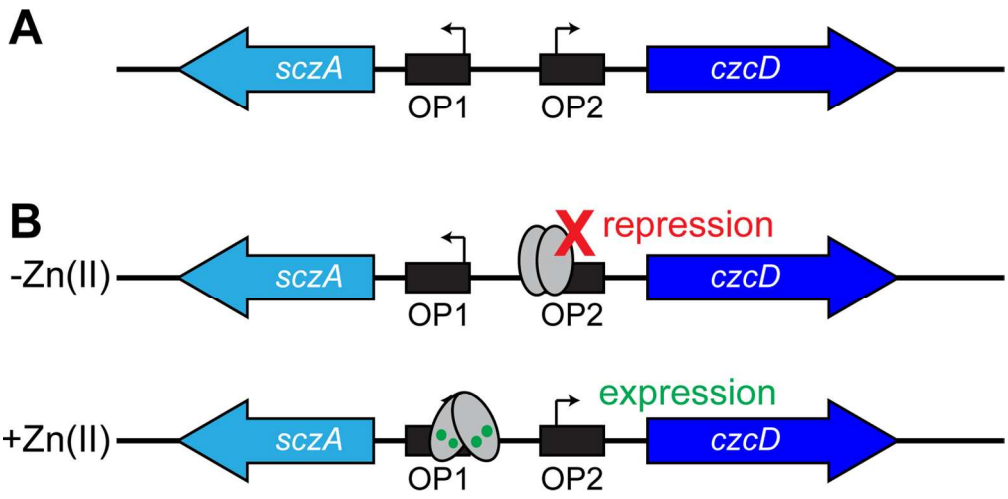

Figure 1
Figure 1
134x64mm (300 x 300 DPI)

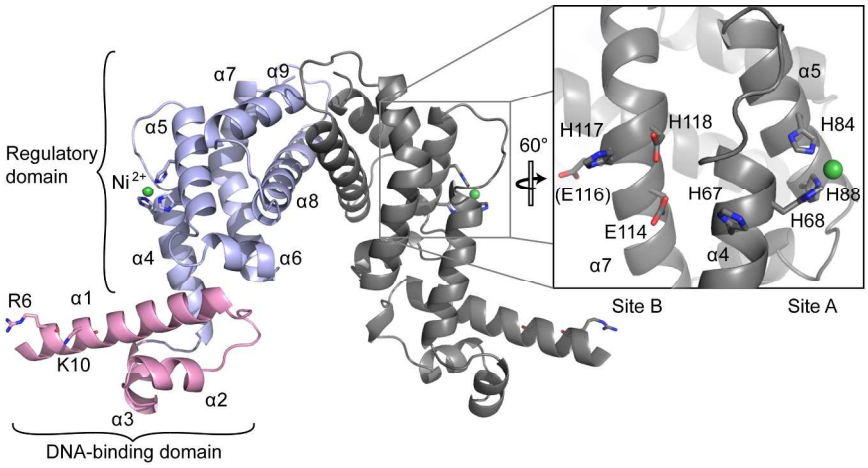

Figure 2
Figure 2
221x101mm (300 x 300 DPI)

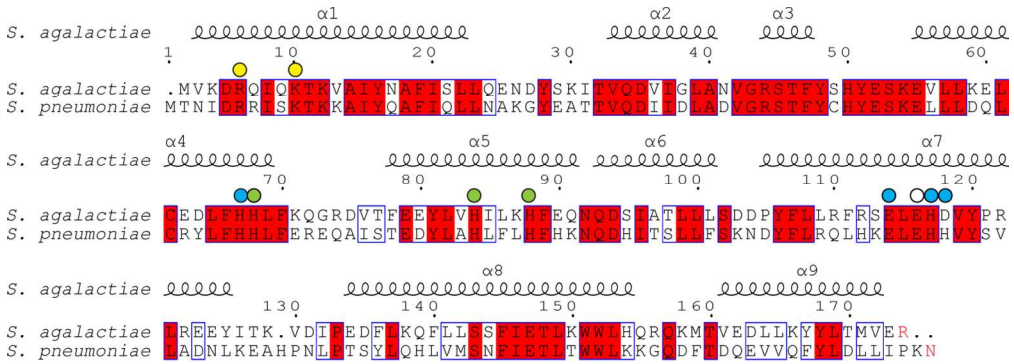

Figure 3
Figure 3
132x46mm (300 x 300 DPI)

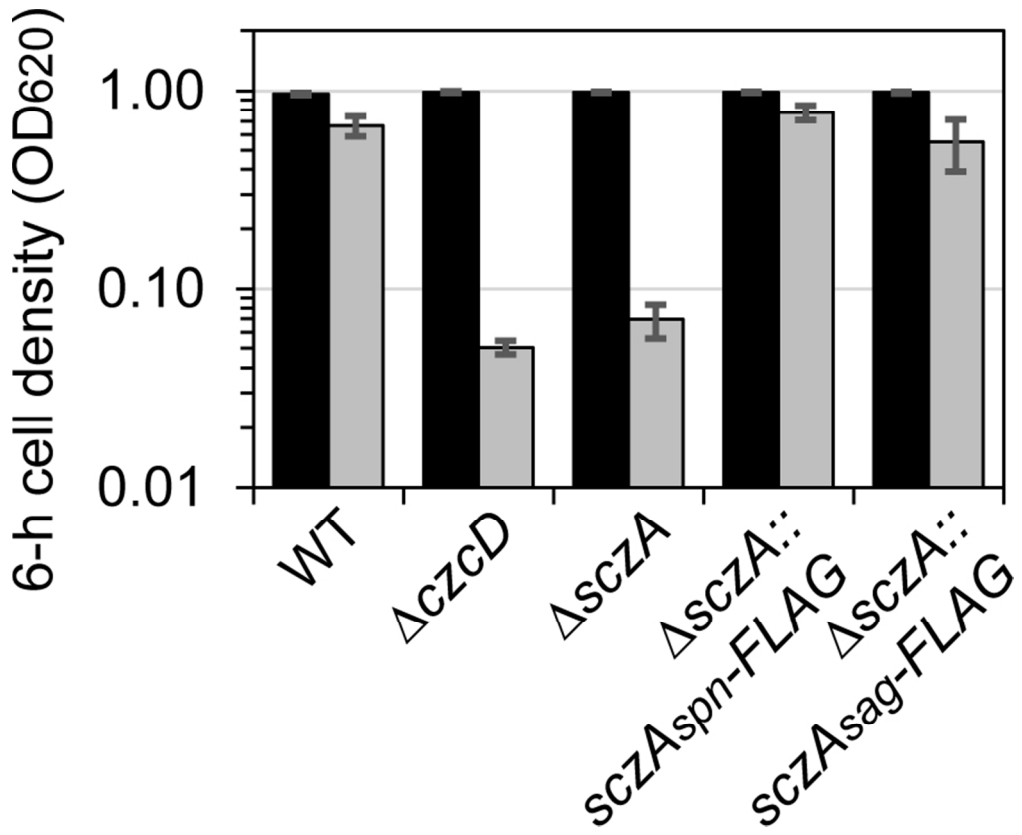

Figure 4
Figure 4
76x62mm (300 x 300 DPI)

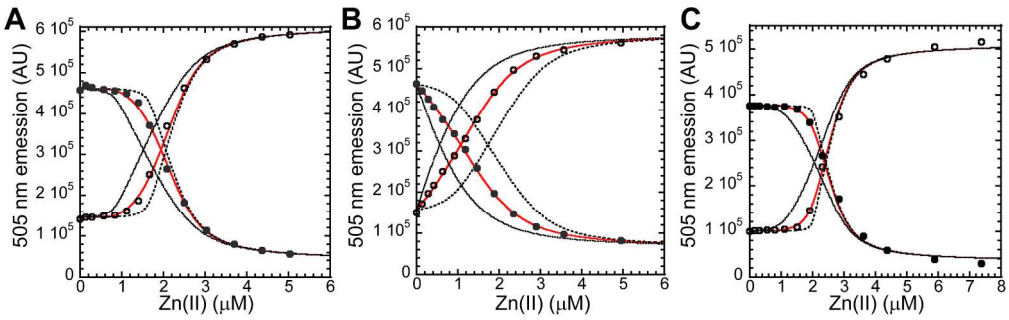

Figure 5
Figure 5
211x64mm (300 x 300 DPI)

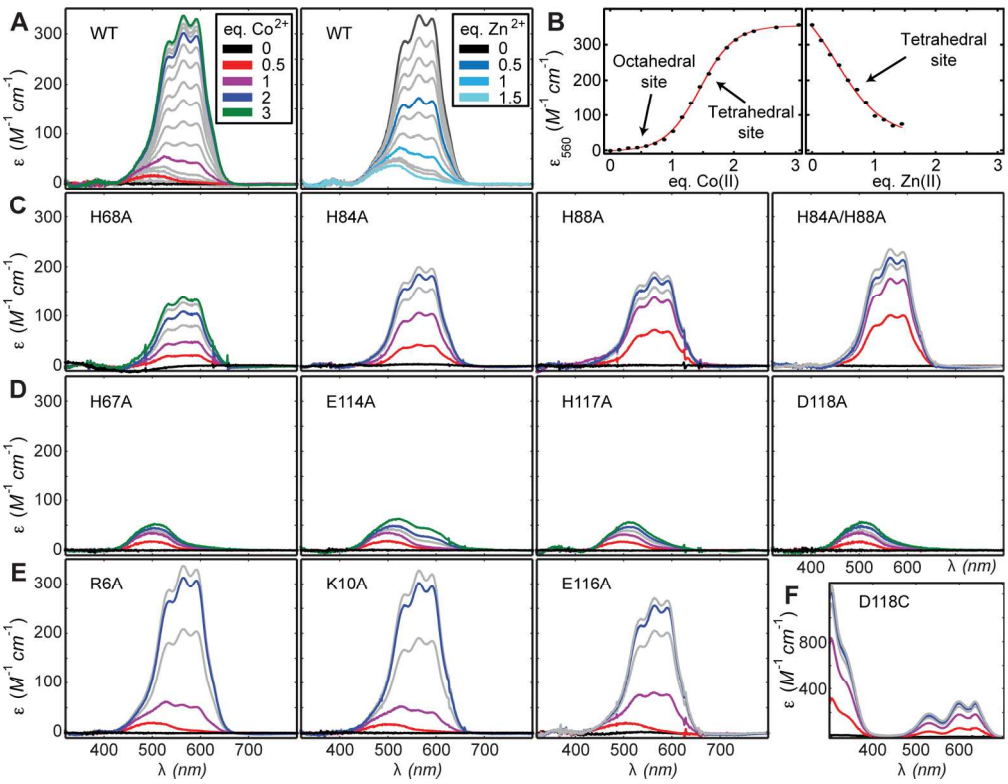

Figure 6
Figure 6
167x128mm (300 x 300 DPI)

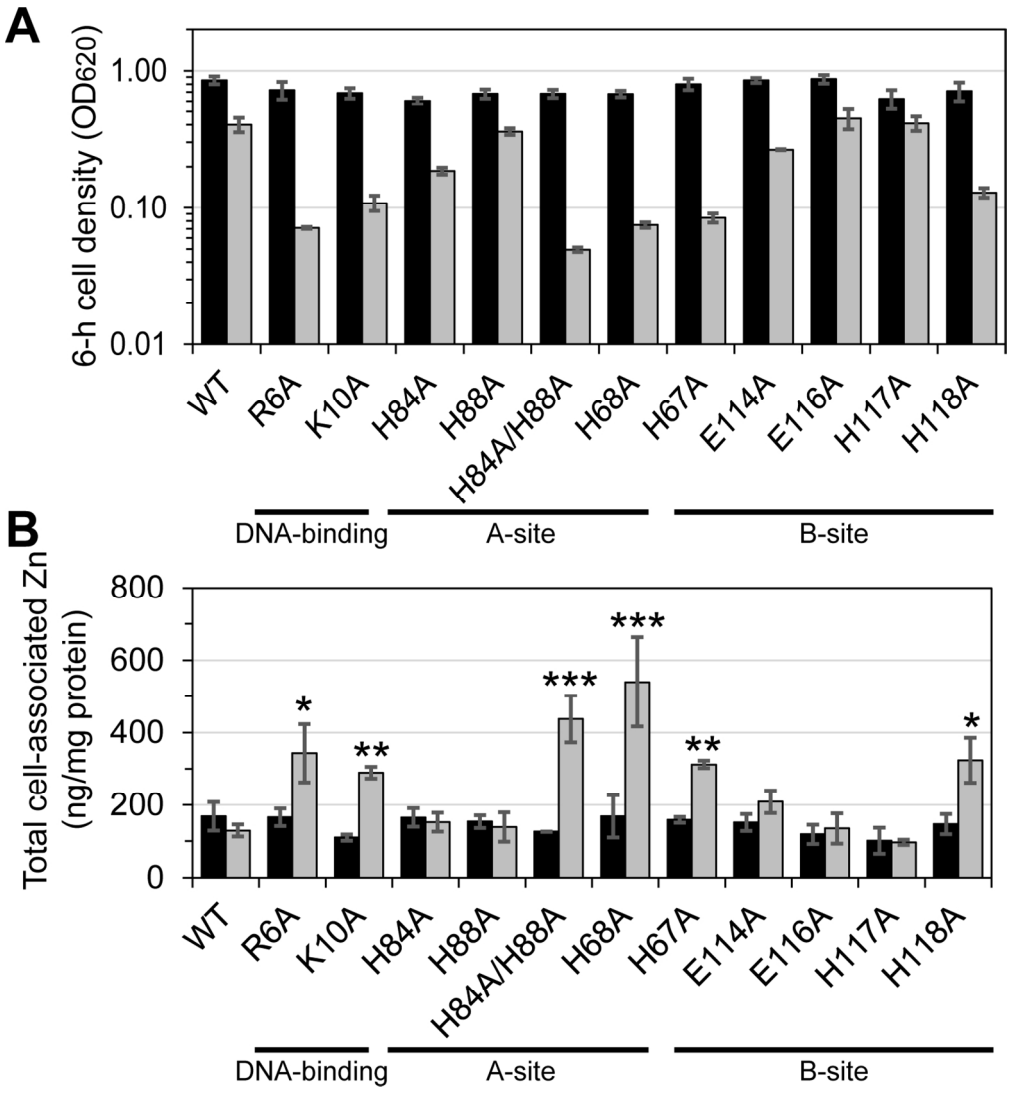

Figure 7
Figure 7
130x140mm (300 x 300 DPI)

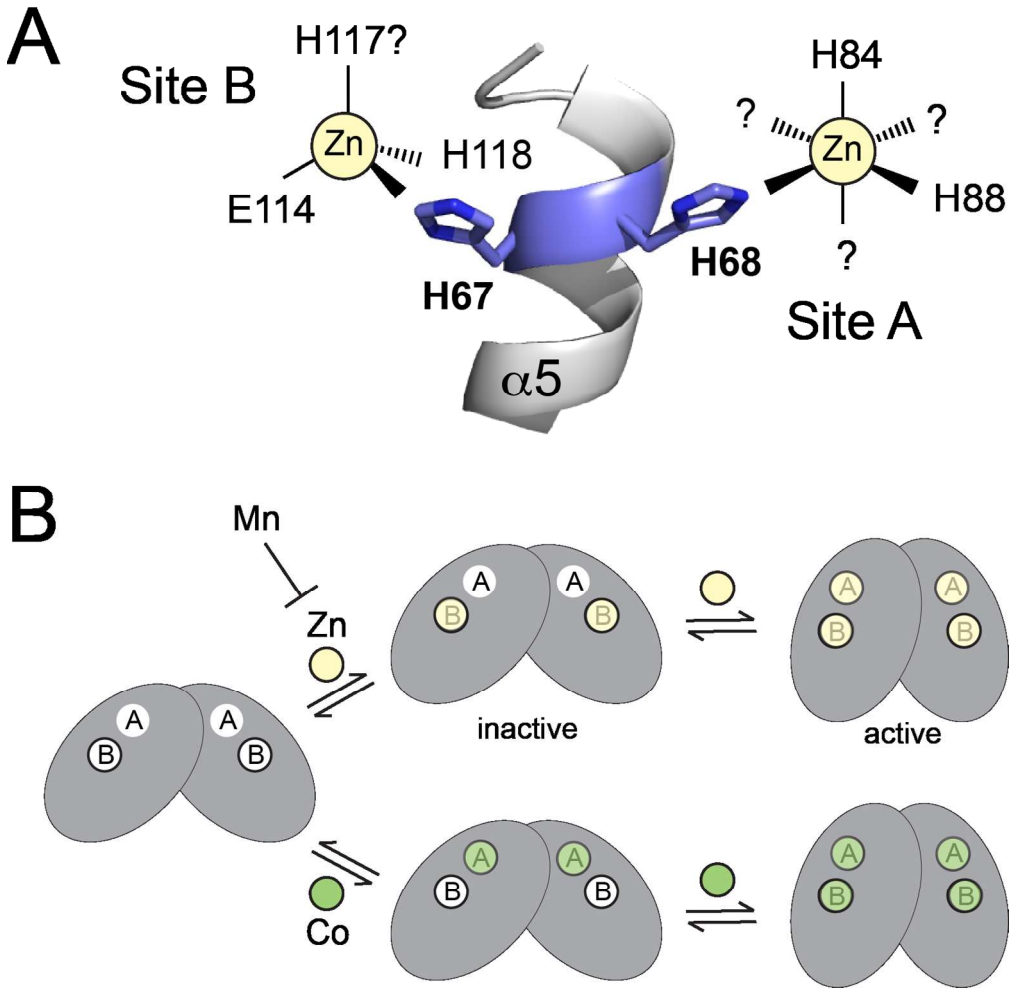

Figure 8
Figure 8

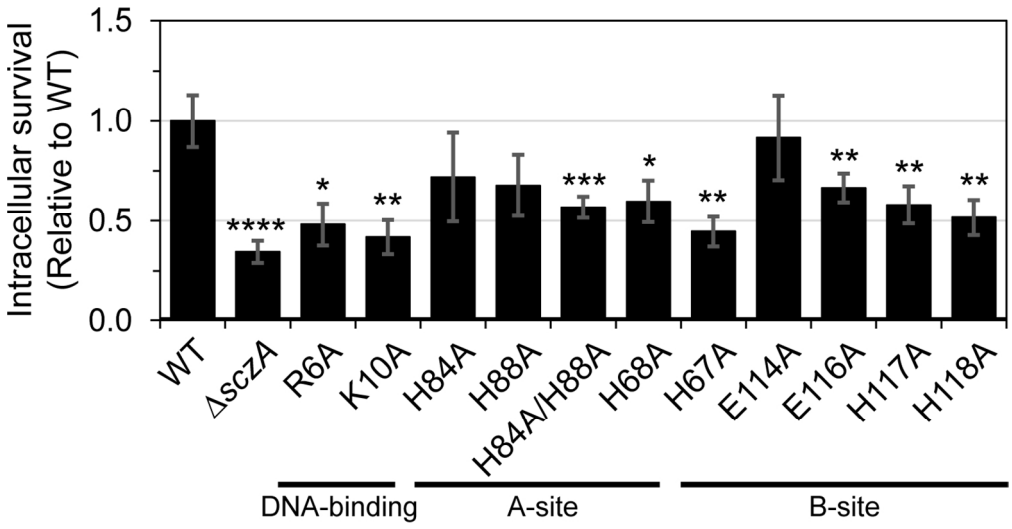

Figure 9
Figure 9
126x65mm (300 x 300 DPI)

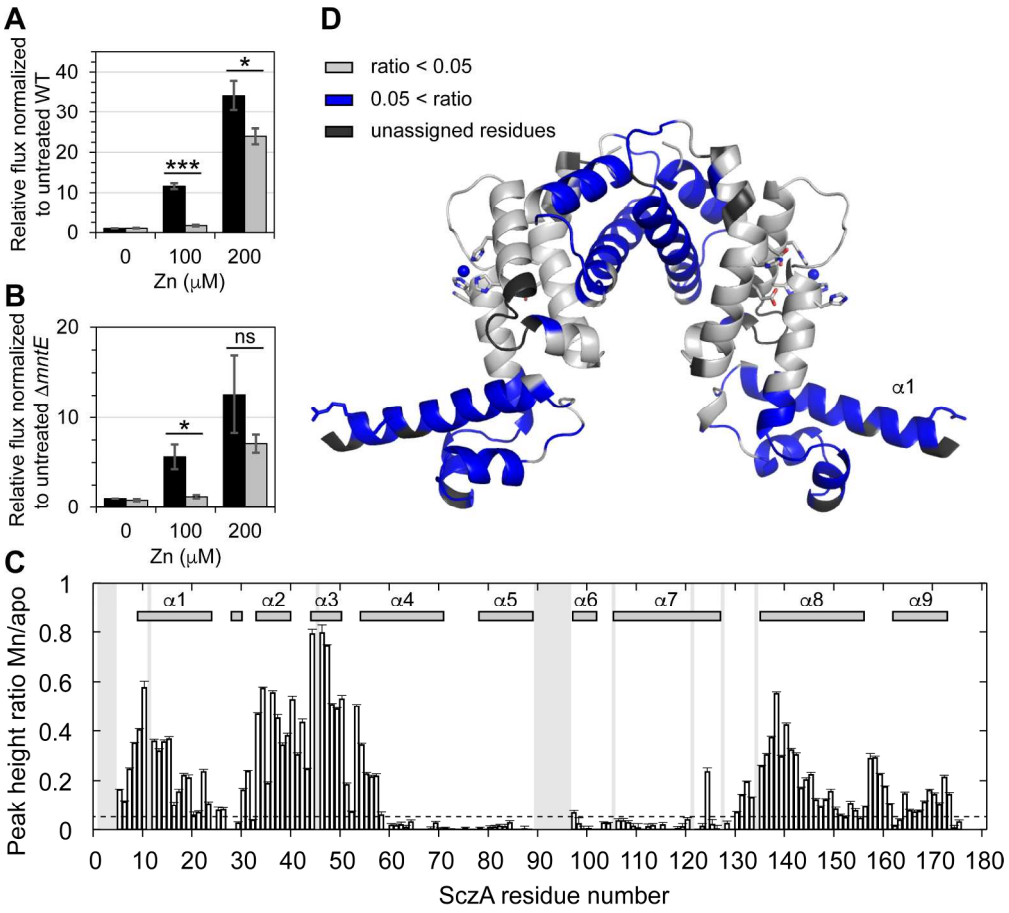

Figure 10
Figure 10
209x187mm (300 x 300 DPI)

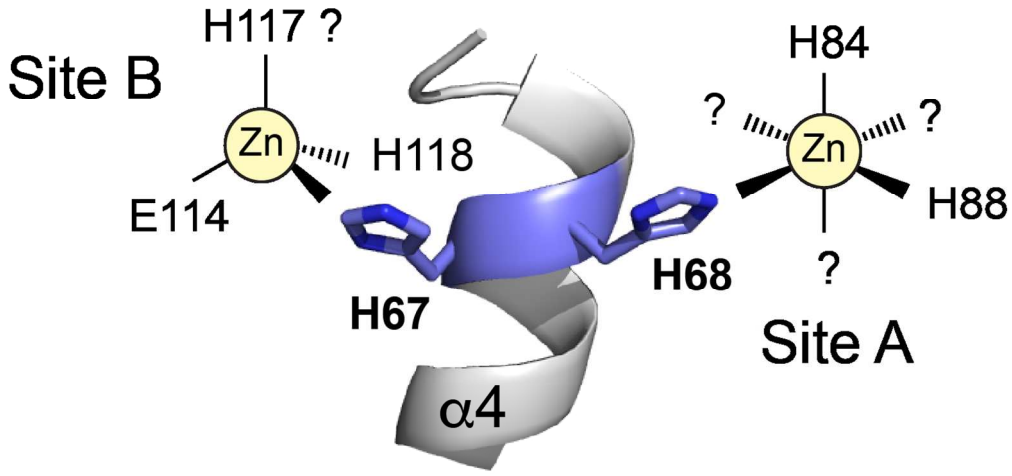

Graphical Abstract
Graphical abstract

How zinc bioavailability triggers activation of the pneumococcal zinc sensor SczA is unknown. Here, we leverage an unannotated x-ray structure of a *bona fide* SczA from *Streptococcus agalactiae* to show that *S. pneumoniae* SczA harbors two distinct metal binding sites, termed A and B, positioned on opposite sides of the C-terminal regulatory domain. Both A- and B-sites are required for resistance against zinc toxicity in both liquid culture and in infected macrophages, likely operative at the host-pathogen interface.